

Influence of capillary absorption and roughness of ceramic substrates on the adhesion of cement pastes

Influência da absorção capilar e da rugosidade de substratos cerâmicos na resistência de aderência de pastas cimentícias

Camila Werner Menegotto 
Monique Palavro Lunardi 
Daiana Metz Arnold 
Leandro Tonietto 
Valéria Costa de Oliveira 
Marlova Piva Kulakowski 
Claudio de Souza Kazmierczak 

Abstrac

This study assesses the joint influence of capillary absorption and substrate roughness on the adhesive strength of a cementitious matrix on brick substrate. One cementitious rendering and two substrates with different water absorption and roughness were used. The capillary absorption coefficient and the roughness coefficient were determined in 1 cm² test areas to then evaluate the matrix tensile bond strength and correlate it with the properties of the substrates. The results were validated by SEM and AFM analyses. Substrates with higher capillary absorption and lower roughness presented higher tensile bond strength. Micro and nanoscale analyses led us to conclude that, in the substrates used, the higher capillary absorption and the lower roughness generate a denser and less porous paste-substrate interface, suggesting a higher extent of contact between the hydrated paste and the substrate and, consequently, higher adhesive strength.

Keywords: Tensile bond strength. Roughness. Capillary absorption. Paste-ceramic substrate interaction.

Resumo

Este estudo avalia a influência conjunta da absorção capilar e da rugosidade do substrato na adesão de uma matriz cimentícia em um bloco cerâmico. Foram usados um revestimento cimentício e dois substratos com absorção de água e rugosidade diferentes. O coeficiente de absorção capilar e o coeficiente de rugosidade da superfície foram determinados em áreas de teste de 1 cm², sendo correlacionados com a resistência de aderência. Os resultados foram validados por análises de MEV e MFA. Os substratos com maior absorção capilar e menor rugosidade apresentaram maior resistência à tração. As análises em micro e nanoescala permitem concluir que, nos substratos utilizados, a maior absorção capilar e a menor rugosidade geram uma interface pasta-substrato mais densa e menos porosa, sugerindo uma maior extensão de contato entre a pasta hidratada e o substrato e, conseqüentemente, maior resistência de aderência.

Palavras-chave: Resistência de aderência, Rugosidade, Absorção capilar, Interação pasta-substrato de cerâmica vermelha.

¹Camila Werner Menegotto

¹Universidade do Vale do Rio dos Sinos
São Leopoldo - RS - Brasil

²Monique Palavro Lunardi

²Universidade do Vale do Rio dos Sinos
São Leopoldo - RS - Brasil

³Daiana Metz Arnold

³Universidade Feevale
Novo Hamburgo - RS - Brasil

⁴Leandro Tonietto

⁴Universidade do Vale do Rio dos Sinos
São Leopoldo - RS - Brasil

⁵Valéria Costa de Oliveira

⁵Instituto Federal de Educação, Ciência
e Tecnologia
Porto Velho - RO - Brazil

⁶Marlova Piva Kulakowski

⁶Universidade do Vale do Rio dos Sinos
São Leopoldo - RS - Brasil

⁷Claudio de Souza Kazmierczak

⁷Universidade do Vale do Rio dos Sinos
São Leopoldo - RS - Brasil

Recebido em 20/12/22
Aceito em 02/05/23

Introduction

The efficiency and durability of mortar coatings depend on various factors such as the mortar's characteristics, substrate properties, weather conditions, and application techniques (COSTA; CARDOSO; JOHN, 2016; CULTRONE *et al.*, 2004; VAZ; CARASEK, 2019). The heterogeneity of both ceramic and mortar materials is well known due to the variability in the raw materials used and the manufacturing methods used (RAMIREZ *et al.*, 2021). This variability in material properties and variations associated with the test methods adopted to determine the adhesive strength affect the variability of adhesive strength (CARASEK; VAZ; CASCUDO, 2018; RAMIREZ *et al.*, 2021; SANTOS *et al.*, 2020; TORRES; VEIGA; FREITAS, 2018; VALENTINI *et al.*, 2022; ZANELATO *et al.*, 2019).

In terms of adhesion strength, multiple mechanisms influence its behavior, including chemical and physical bonds at atomic and molecular levels, mechanical forces at the nano and microscale, and the extent of contact, which refers to defects at the macroscale (COSTA; CARDOSO; JOHN, 2017; KENDALL, 2001; PAES *et al.*, 2014; SHULTZ; NARDIN, 2003). While numerous studies have been conducted on mortar composition, mechanical properties, and durability (GONZÁLEZ-SÁNCHEZ *et al.*, 2021; HAN *et al.*, 2015; HUANG *et al.*, 2021; KAZMIERCZAK; ROSA; ARNOLD, 2016; PALOMAR; BARLUENGA, 2018; SENTENA; KAZMIERCZAK; KREIN, 2018; STOLZ; MASUERO, 2018), the influence of the substrate on adhesive strength requires further investigation (ARNOLD *et al.*, 2021; THAMBOO; DHANASEKAR, 2015; VALENTINI *et al.*, 2022; VAZ; CARASEK, 2019). Likewise, despite being a multiscale property, bond strength is mostly measured on a macroscale, and there is a need to better understand its behavior across different scales.

The adhesion of mortar to a ceramic substrate is significantly influenced by the surface roughness and water absorption properties of the ceramic blocks (BARRIOS-MURIEL *et al.*, 2019; GROOT; LARBI, 1999; PAES *et al.*, 2014). These properties are determined by the raw material properties and the manufacturing process of the blocks (AZEVEDO *et al.*, 2018). The manufacturing process, including clay mineralogical composition, extrusion, the heating-drying process, and industry quality control, influences the porous system, mechanical properties, and variability of the blocks (AÏT OUMEZIANE *et al.*, 2021; RAMIREZ *et al.*, 2021). The substrate's pore structure affects the ceramic block's pore connectivity and capillary force characteristics. These factors, in turn, impact the movement of water between the substrate and mortar, resulting in an instantaneous change in the water/binder ratio on the interface zone (KAHANGI SHAHREZA; NIKLEWSKI; MOLNÁR, 2021; MONTEIRO; MASO; OLLIVIER, 1985; ZUO; XIAO; YUAN, 2020). Depending on the block humidity and the pore system of the block and mortar, the mortar can either lose or absorb water (DETRICHE *et al.*, 1985; DUPIN; DETRICHE; MASO, 1988).

The adhesion between mortar and substrate is influenced by the extent of contact between them (SARKER; DIAS-DA-COSTA; HADIGHEH, 2019), which is smaller than the apparent contact area (COUTO CARNEIRO; PINTO CARVALHO; ANDRADE PIRES, 2020). The roughness of the ceramic block surface is an important property that affects adhesion, determined by the shape and dimensions of the peaks and valleys on the substrate surface (BARRIOS-MURIEL *et al.*, 2019; VENKATARAMA REDDY; LAL; NANJUNDA RAO, 2007). Typically, an increase in roughness results in an increase in the extent of contact. However, if the depth of the valleys is smaller than the particle size of the materials in the mortar, this effect can be reversed (HOŁA *et al.*, 2015; LI *et al.*, 2020; VAN DAM *et al.*, 2020; WANG *et al.*, 2014).

Despite the crucial role of substrate roughness in determining the efficiency of adhesion between two materials, widely accepted standards such as BS 3921 (BRITISH..., 1985), C67 (AMERICAN..., 2013), EN 771-1 (BRITISH..., 2011), and NBR 15270-1 (ABNT, 2017) do not include roughness as a parameter for evaluation. There is currently no clear definition for assessing roughness parameters in ceramic substrates (TONIETTO *et al.*, 2022), and the scale of analysis significantly impacts the roughness measurements (YANG; PERSSON, 2008). For ceramic substrates, the roughness should be analysed at the micrometer and/or nanometer scale to match the particle size of the mortar and establish a peak-valley relationship with the particle diameter (COSTA; CARDOSO; JOHN, 2016). Traditionally, studies on roughness have relied on two-dimensional profiles generated from peak and valley tracing along a single cross-section of the substrate (KOZUBAL *et al.*, 2020). However, this approach does not allow the assessment of the number of peaks and valleys, which is essential for establishing a relationship between roughness parameters and mortar-substrate adhesion. Recent studies have proposed a more advanced method for roughness analysis, which involves generating roughness signatures through three-dimensional analysis at the micrometer level (ARNOLD *et al.*, 2021; TONIETTO *et al.*, 2019).

Recently, there has been growing interest in the application of multiscale techniques to gain a better understanding of the behavior of construction materials. However, there has been little discussion of using such techniques to evaluate bond strength mechanisms of rendering mortars. This study presents a novel approach to quantitatively relate substrate properties (roughness and capillary absorption) with the tensile bond strength of cement paste. This is achieved by measuring all three properties within the same area of analysis and using test methods specifically designed for this purpose to minimise the impact of confounding factors that can lead to excessive variability in such studies. Moreover, the correlation hypothesis between the properties is validated through interface analysis techniques at the micro and nanoscale.

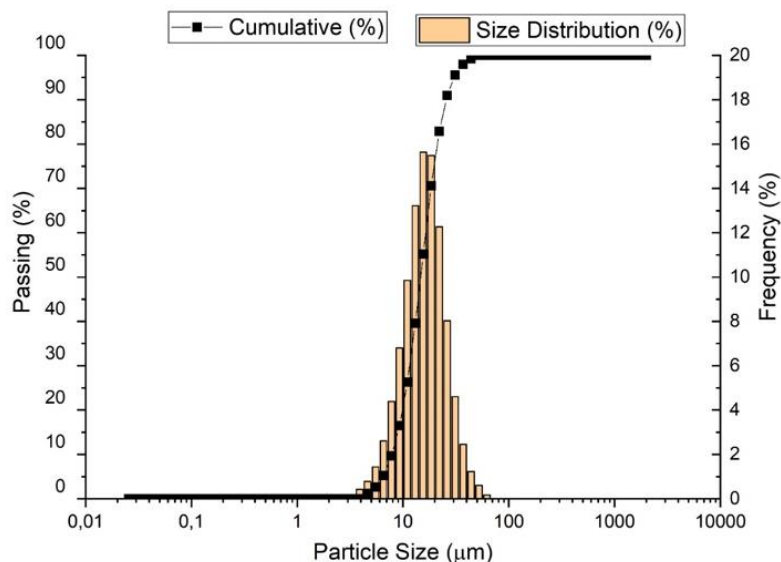
Materials

The study involved applying a cementitious paste on two different types of red ceramic substrates, in small square areas measuring 10mm in edge length and 5mm in height, where the average roughness and capillary water absorption were previously determined. Ceramic substrates were selected with differences in capillary absorption and roughness. After curing in a saturated environment for 28 days, adhesion tests were conducted in each of these areas. Microstructural tests, such as scanning electron microscope (SEM) on the interface between cement/substrate at the microscale, and atomic force microscope (AFM) in nanoindentation mode to indent the substrate surface and interface at the nano and microscale, as well as optical microscopy, were used to evaluate the interface regions between the binder and the substrate. The definition of small test areas was due to the intention of minimising the variability of the tests (TONIETTO *et al.*, 2019) and resulted in the need to adapt the characterisation and adherence tests to these dimensions.

The cement paste was produced with Brazilian Portland Cement type V – ARI, at a water/cement ratio of 0.4, with 0.4% of an air-detraining admixture. This process was necessary to guarantee maximum contact between the cement paste and the ceramic, as the contact area is small, and a void would negatively impact adhesion strength. The grain size distribution of the cement (Figure 1) was characterised by laser granulometry Microtac model S3000/S3500 using isopropyl alcohol as dispersant, resulting in $D_{10} = 7.89\mu\text{m}$, $D_{50} = 14.72\mu\text{m}$, and $D_{90} = 25.53\mu\text{m}$.

Two different red ceramic plants were chosen to obtain red ceramic substrates with varying capillarity coefficients and roughness.

Figure 1 - Grain size distribution of the cement



The roughness of each 10 mm x10 mm area to be coated was determined using a three-dimensional laser profilometer, LiDAR (Starrett, AV300+) with X and Y resolution of $E2 = 1.9 \mu\text{m} + 5L/1000$ and Z resolution of $E1 = 2.5 \mu\text{m} + 5L/1000$, with a scale resolution of $0.1 \mu\text{m}$. Each surface was scanned in the X, Y, and Z axes using the methodology described by Arnold *et al.*, 2021, and Tonietto *et al.*, 2019. The average roughness coefficients Ra of each region was determined as proposed by Tonietto *et al.* 2019. This method performs a computational process, with the point cloud as input information for each sample. The system aims to compute average roughness in several regions of each sample (with spatial subdivision) so that it is possible to perform a qualitative and quantitative analysis of roughness in a localised way and with greater detail. Thus, roughness coefficients for each subarea can be obtained, in addition to the general average roughness of the sample, and, by doing this, the roughness behavior can be verified throughout the sample. The main difference between this method and the results of two-dimensional approaches (which are the most used) is that it generates a roughness coefficient that is more representative of the substrate as the direction of the line, in two-dimensional methods, can change the value of the roughness coefficient substantially (ARNOLD *et al.*, 2021). A point cloud was obtained by processing approximately 10,000 points (X, Y) in each analysis region. As this number of points is close to the data acquisition limit allowed by the equipment, and due to the roughness being determined on a micrometric scale, it has conditioned the maximum size of the area to be evaluated, resulting in dimensions of 10 mm x 10 mm (X, Y).

Methods

Mechanical tests

In order to ensure the precise application of the coating in the same areas where roughness was evaluated, a template (Figure 2) was utilised. However, due to the small size of the area, capillary absorption was analysed on larger sample pieces.

The capillary absorption was performed according to RILEM TC 116 PDC (WILSON; CARTER; HOFF, 1999) in two samples per block, on the face that received the coating. The sample's weight was measured at 1 min, 2 min, 5 min, 10 min, 20 min, 30 min, 60 min, 2 h, 6 h, 24 h, 72 h, and 7 days (VALENTINI, 2018), from which the capillarity coefficients $((\text{g}/\text{cm}^2) \cdot \text{h}^{1/2})$ were calculated.

The methodology adopted for the paste mixing followed the sequence described in NBR 16606 (ABNT, 2018) and C150/C150M (AMERICAN..., 2009). The paste consistency, determined by the Kantro mini-slump test (RAUCCI *et al.*, 2018), was 70 ± 1 mm. The fresh state paste showed a density of $1.72 \text{ g}/\text{cm}^3$ measured by the equation m/v , based on NBR 13278 (ABNT, 2005). For the paste characterisation, cylindrical specimens measuring 15 mm x 30 mm were molded for axial compressive strength tests, according to NBR 7215 (ABNT, 2019) and C39/C39M (AMERICAN..., 2016), and tensile strength by diametral compression, according to NBR 7222 (ABNT, 2011). The dimension of the sample is smaller than that required by the standard, however the 2:1 proportion was maintained. The authors opted for a smaller sample due to the tendency of the paste to shrink and segregate in larger dimensions.

The axial compressive strength obtained (average value of six specimens) was 61.66 MPa, with a standard deviation of 1.81 MPa, and the average diametral compression tensile strength was 8.83 MPa, with a standard deviation of 1.71 MPa. In order to ensure adequate adhesive strength and to direct the ruptures resulting from the tensile strength test to the paste-substrate interface region, a paste with high mechanical strength was used.

The coating application on the substrates was carried out in the same areas where each roughness was determined. Specimens whose coating, carried out with the paste, showed dimensions of 10 mm x 10 mm edge and 5 mm height were molded. The application was performed by free fall, with a launch height of 80 mm and subsequent application of a confinement load of $83.0 \text{ g}/\text{cm}^2$ in each 10 mm x10 mm area to simulate the impact energy in a real application as the dimensions are reduced and only the folder's weight would not have enough energy to keep in contact and simulate the real situation (Figure 2). The specimens remained for 28 days in a saturated environment with a humidity of $95\% \pm 5\%$ and a temperature of $23 \pm 2 \text{ }^\circ\text{C}$.

After curing, the tensile bond strength of the coatings was determined. The test, according to NBR 15258 (ABNT, 2016) and EN 1015-12 (BRITISH..., 2000) standards, must be performed in a circular area, with a diameter of 50 mm. However, considering that this study aims to assess the influence of substrate properties on adhesive strength, and that ceramic substrates are strongly heterogeneous (AZEVEDO *et al.*, 2018; BARRIOS-MURIEL *et al.*, 2019; CULTRONE *et al.*, 2004; RAMIREZ *et al.*, 2021), and that the areas where the roughness of the substrates was determined were square (10 mm x 10 mm), this shape and dimension were adopted for the adhesion resistance tests. The methodology developed to carry out the tensile bond strength

test in reduced areas, of 1 cm², presented a coefficient of variation 2%, based on previously performed tests (Figure 3), lower than that usually obtained in the test standardised by NBR 15258 (ABNT, 2016). The calculation of adhesion strength was based on the applied tension force divided by the analysis area, considering 1cm².

Microscale analysis

The analysis at the micrometric level was performed using SEM (Zeiss, EVO MA 15) with a resolution of 1 nm, coupled to an energy dispersive spectroscope and it was operated with an accelerating voltage of 15 kV and 8 mm distance. After 28 days of curing, a cross-section was carried out on the samples, generating specimens with dimensions of 10 mm x 10 mm x 3 mm, which allowed the visualisation of the paste-substrate interfaces from the specimens molded for the tensile bond strength tests (Figure 4). The hydration was interrupted with isopropyl alcohol (AVET; LI; SCRIVENER, 2018). Afterwards, the samples were dried in an oven at 40 °C (at temperatures above 40 °C, water is lost, which is combined with other cement hydration products) for 24 h and embedded with acrylic resin. The samples were polished with silicon carbide sandpaper in grammage 240, 320, 400, 500, 600, and 1200, and finished with 0.3 µm diamond paste and isopropyl alcohol. The samples were dried in an oven at 40°C for 24 hours and metalized with gold.

The analyses at the nanometric level were performed using AFM. The same sample preparation process for the SEM was used, except for the absence of the metallization process. An AFM (NT-MDT, Solver Next) was used, with a silicon tip with the following dimensions: T = 2.5 ± 0.5 µm, W = 32 ± 3 µm, and L = 225 ± 5 µm, with a typical resonance of 60 kHz, and a force constant of 3 N/m. The analyses were carried out in contact mode, to obtain sample amplitude, phase contrast, and topography maps. Before the AFM tests, the same samples were visualized in an optical microscope with a 10 times magnification, to visualise the quality of the paste-substrate interfaces polished sections.

Figure 2 - Pictures of the molding procedure



Figure 3 - Methodology for testing tensile bond strength

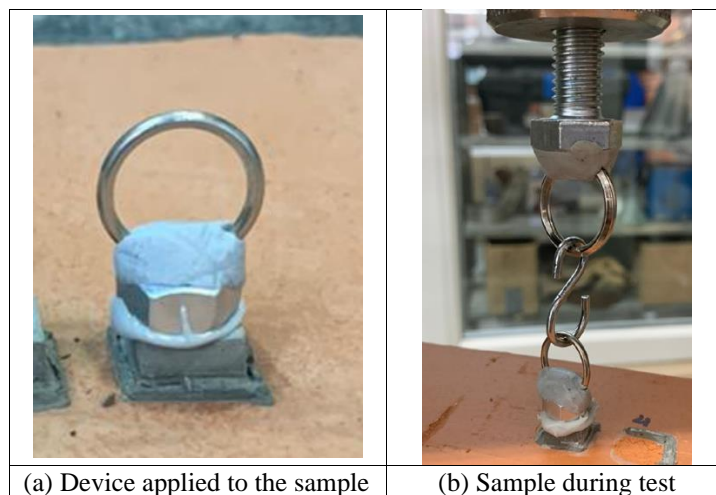
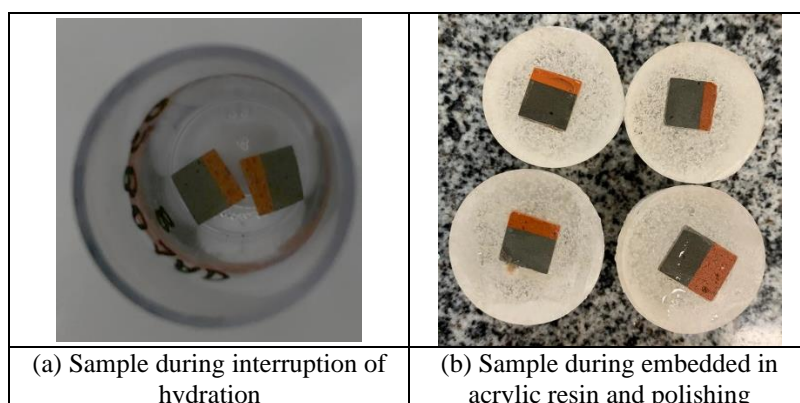


Figure 4 - Samples for AFM and SEM tests



For the AFM analysis, 3 measurement areas were selected on the paste-ceramic interface, 3 areas on the paste, and 3 areas on the ceramic. The analysis areas were $50 \times 50 \mu\text{m}$, with a reading of 550×550 points, resulting in an accuracy of 8 nm. Within the analysis areas, indentations were made and, from force curves versus displacement, the modulus of elasticity (E) were calculated.

The modulus of elasticity was calculated using Equation 1, modeled for conical tips, where α is the semi-angle of the tip cone, in radians (18° for NT-MDT tips), ν is the Poisson's ratio of the material, 0.3 for the paste, and 0.13 for the ceramic (FOUCHAL; LEBON; TITEUX, 2009), F is the force used to indent and δ is the indented depth.

$$E = \frac{\pi}{2-tg(\alpha)} \cdot \frac{\Delta F}{\Delta \delta^2} \cdot (1 - \nu^2) \quad \text{Eq. 1}$$

It should be noted that the modulus of elasticity obtained on a macroscale from static tests is determined by considering the deformation of a specimen because of the load applied to it. At the nanoscale, however, the modulus of elasticity of each indentation point in the sampled area is determined (in this research, areas of $50 \times 50 \mu\text{m}$ were adopted), and the average modulus of elasticity of the specimen is estimated to be the highest point of the distribution curve.

Results and discussion

The results of the substrate characterisation tests are summarised in Table 1.

The maximum capillary force observed in substrates occurs between 10 and 30 minutes from the first contact with water, given the high porosity of ceramics (AZEVEDO *et al.*, 2018; CULTRONE *et al.*, 2004; GROOT; LARBI, 1999; PAES *et al.*, 2014; VALENTINI, 2018). Substrates 1 and 2 showed average capillarity coefficients of $0.83 \text{ g/cm}^2 \cdot \text{h}^{1/2}$ and $0.50 \text{ g/cm}^2 \cdot \text{h}^{1/2}$, respectively. The analysis of variance (at a significance level of 5%) indicated significant differences in capillarity between the substrates, which meets the initial research hypothesis of adopting two substrates with different capillarity coefficients. Substrate 1 showed the highest total water absorption (WA), coinciding with the highest capillarity coefficient.

Figure 5 presents the frequency distribution of the modulus of elasticity obtained by nanoindentation of the two substrates.

Substrate 1 showed a higher frequency of values up to 12 GPa, considered by several authors (CONSTANTINIDES; ULM, 2007; SORELLI *et al.*, 2008) as a typical modulus of elasticity of indentations on micropores and macropores. Thus, it is estimated that this substrate also has the lowest modulus of elasticity in tests on a macroscopic scale.

The modulus of elasticity results support what was observed in the total water absorption test, indicating that Substrate 1, in addition to having the highest water absorption, has the lowest elasticity.

The average roughness (μm) of each substrate is shown in Figure 6.

Substrates 1 and 2 showed average roughness of $1.12 \mu\text{m}$ (CV = 71%), and $2.35 \mu\text{m}$ (CV = 16%), respectively. Roughness is influenced by the composition of the ceramic mass and the ceramic manufacturing process, mainly by the firing and cooling temperatures (AZEVEDO *et al.*, 2018; CULTRONE *et al.*, 2004; PINHEIRO; HOLANDA, 2010).

Table 1 - Total absorption, capillary absorption, and modulus of elasticity by AFM of the two substrates

Block type	Water Absorption (WA) (%)	Capillarity Coefficient (g/cm ² .h ^{1/2})	Modulus of Elasticity (GPa) by AFM
1	17.95 (CV 7%)	0.83 (CV 13%)	26 (CV 26%)
2	11.37 (CV 8%)	0.50 (CV 20%)	31 (CV 19%)

Note: CV - Coefficient of variation.

Figure 5 - Frequency distribution of Modulus of Elasticity obtained by indenting substrates

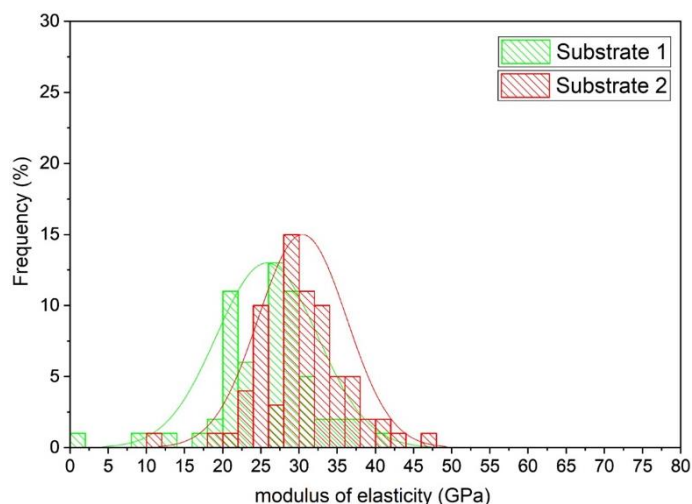
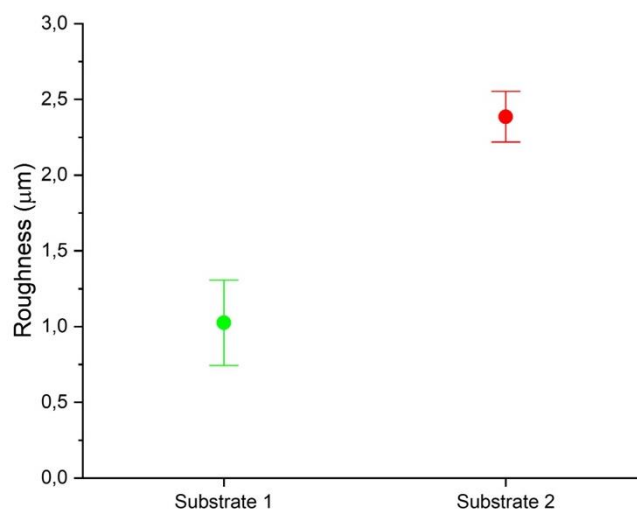


Figure 6 - Average roughness and standard deviation of Substrates 1 and 2



The variability of the roughness results is explained by the heterogeneity of the ceramic material and by increasing the scale of analysis (YANG; PERSSON, 2008). Statistical analysis of variance indicated that the substrates have significantly different roughness.

Although roughness and capillary absorption are considered interdependent properties, in this research they were inversely proportional as substrates with higher capillary absorption have lower roughness. When comparing two substrates from different clay masses, there may not be a direct relationship between the properties among them. It is also relevant to consider that in different manufacturing processes, clay compaction and subsequent firing can result in a smoother surface for one of the substrates, with smaller and connected pores, and consequently high capillary strength. In addition, on a less rough surface, the contact of water with the internal pores is direct, that is, there are no obstacles for water to penetrate the pores (BARRIOS-MURIEL *et al.*, 2019; LI *et al.*, 2020).

The adhesive strength observed between the cementitious matrix and the substrates is shown in Figure 7.

The substrates showed statistically different means, that is, 1.12 MPa (CV = 19%), and 0.85 MPa (CV = 35%) for Substrates 1 and 2, respectively. The analysis of variance indicated that the substrates have significantly different tensile bond strength. Tensile bond strength shows high variability, which can be observed in some studies (CARASEK; VAZ; CASCUDO, 2018; VAZ; CARASEK, 2019). It is estimated that the high coefficients of variation found in capillary absorption and roughness are factors that corroborate for this variability.

Table 2 shows the influence of capillarity and roughness on the tensile bond strength of the set.

By correlating the properties, it was observed that the capillarity coefficient and the tensile strength showed a directly proportional behavior; that is, with the increase in the capillarity coefficient, there is an increase in the tensile bond strength (BERNARDO *et al.*, 2020), as the force caused by the capillary pressure increases the proximity of the cement grains with the rough surface of the substrate, decreasing the liquid-vapor (VERPLANCK *et al.*, 2007) and also changing the w/c ratio on the interface. However, analysing the relationship between roughness (Ra) and tensile bond strength, an opposite behaviour was observed; with increasing roughness, there was a decrease in tensile bond strength. It is estimated that with the increase in roughness, the cementitious paste could not penetrate the more profound valleys (due to inadequate rheological characteristics), creating points of failure and decreasing the contact extension, consequently reducing the bond strength. This effect occurs because the high roughness influences the tensile bond strength of the particles, which can reduce the contact extension if the cementitious paste has inadequate viscosity (THORNTON; CUMMINS; CLEARY, 2017). It is still possible to assume that the liquid does not completely wet the rough surface as air is at the bottom of the valleys. Therefore, there is an interface between liquid-solid and liquid-air, which is responsible for failures in the extension of contact; the steeper the value of the valley, the greater the propensity for this effect (SANJAY *et al.*, 2012; VERPLANCK *et al.*, 2007). The tensile bond strength between the cementitious paste and the substrate decreases with increasing roughness until the size of the peaks and valleys becomes larger or approximate to the size of the paste particles (LI *et al.*, 2020). Therefore, the behaviour found in the analysed specimens cannot be extrapolated to other pastes or substrates as it depends on the relationship between the roughness and the size of the binder particles and the inert used.

Figure 7 - Tensile bond strength average and standard deviation of Substrates 1 and 2

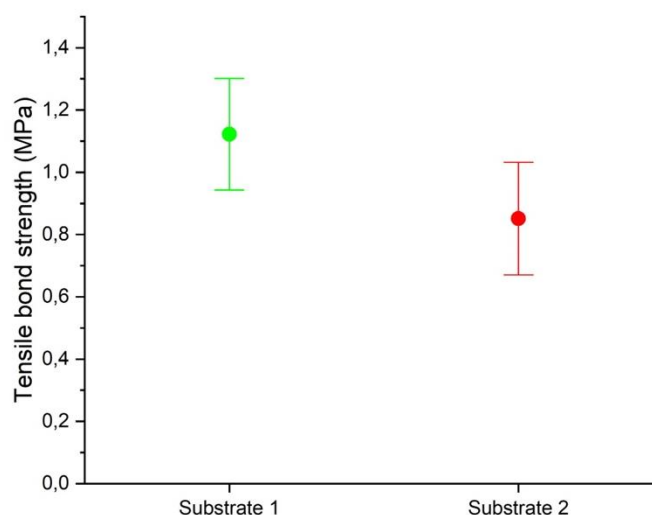


Table 2 - Capillarity coefficient, roughness and tensile bond strength of the two substrates

Sample	Capillarity coefficient (g/cm ² .h ^{1/2})	Roughness (µm)	Tensile bond strength (MPa)
Substrate 1	0,83	1,12	1,12
Substrate 2	0,5	2,35	0,85

Substrate 1 showed the highest capillarity coefficient and the lowest average roughness. Considering that higher capillarity tends to favour adherence and that lower roughness tends to allow higher contact between the paste and the substrate, these two factors contributed to Substrate 1 presenting higher adhesive strength, compared to Substrate 2.

In Substrate 2, which showed lower capillary absorption and roughness about three times higher than that of Substrate 1, there was a decrease in adhesive strength, possibly due to a decrease in the extent of adhesion.

Substrates with higher capillary absorption and lower roughness resulted in greater tensile bond strength (around 1.12 MPa). Conversely, those with higher roughness resulted in lower tensile bond strength (around 0.85 MPa), concluding that the capillarity showed a behaviour directly proportional to the tensile bond strength, which may be linked to the fact that the capillary force causes the cement grains to approach the substrate, reducing failures at the interface. As for roughness, the influence occurred in the opposite direction, where higher roughness resulted in a decrease in tensile bond strength, which is explained by the hypothesis that with a larger valley, there is air in the depressions in addition to cement grain sizes larger than the dimension of the valley, generating contact failures between the materials.

The images (Figure 8) obtained under an optical microscope show the interface between the cementitious matrix and the substrate, as well as points of failure. It should be noted that the specimens (measuring 10x10mm) were sectioned using a precision saw and were not subjected to any additional external forces.

At this visualisation scale, it was noted that Substrate 1 did not show any visible failures in its contact extension. It was estimated that the block's high capillarity and lower roughness contributed to the reduction in contact extension failures. Conversely, failures in the contact extension were observed in Substrate 2, as shown in Figure 8(b). The low tensile bond strength could be attributed to high roughness and low capillarity coefficient, which could have caused water to accumulate at the interface, impeding the interaction between the cementitious paste and the substrate, ultimately leading to failures in the contact extension.

Figure 9, obtained by SEM, presents images of each substrate, where a similar behaviour can be observed to the one shown in Figure 8.

There is a significant difference between the cementitious paste and the interface zone in the two samples. Observing Substrate 1, which presented an average tensile bond strength of 1.12 MPa and an average capillarity coefficient of $0.83 \text{ g/cm}^2 \cdot \text{h}^{1/2}$, it can be observed that this block has higher homogeneity and, apparently, lower porosity. However, based on the high coefficient of capillarity, the pores may be small, but have connectivity, justifying the capillary absorption. The interface zone, with an average thickness of $55 \mu\text{m}$, is visually more compact and less porous than that observed in Substrate 2, which is consistent with their higher tensile bond strength. In Substrate 2, which presented an average tensile bond strength of 0.85 MPa and an average capillarity coefficient of $0.50 \text{ g/cm}^2 \cdot \text{h}^{1/2}$, it can be noted that the interface zone, with an average thickness of $40 \mu\text{m}$, has similar characteristics to those of the cementitious paste, however, the existence of cracks and failures in the contact extension is perceptible.

The modulus of elasticity in the interface region between the hydrated paste and the substrate were determined, on a microscale, using AFM, and their distribution can be seen in Figure 10.

Figure 8 - Paste-ceramic substrate interface region visualised by optical microscopy (10x magnification)

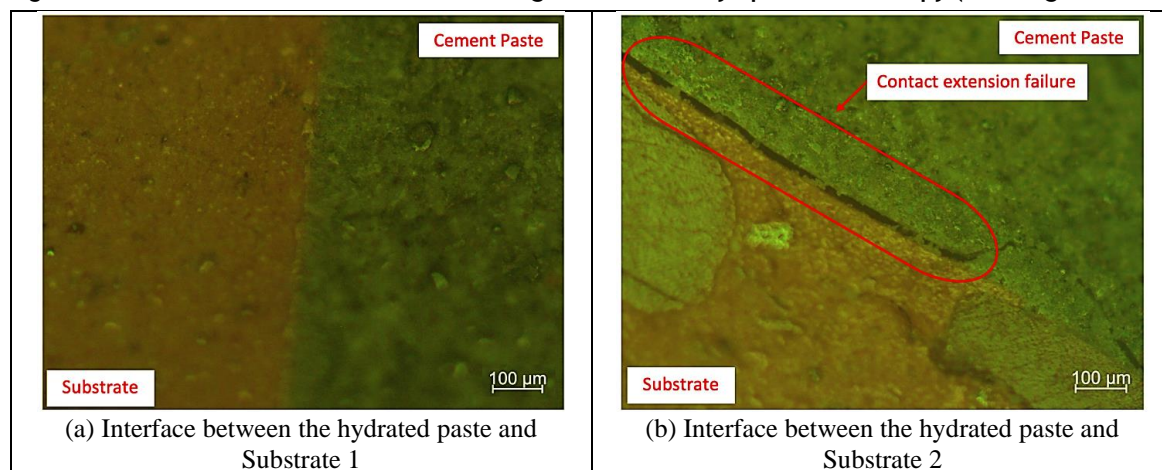


Figure 9 - Paste-ceramic substrate interface region visualised by SEM (500 times magnification)

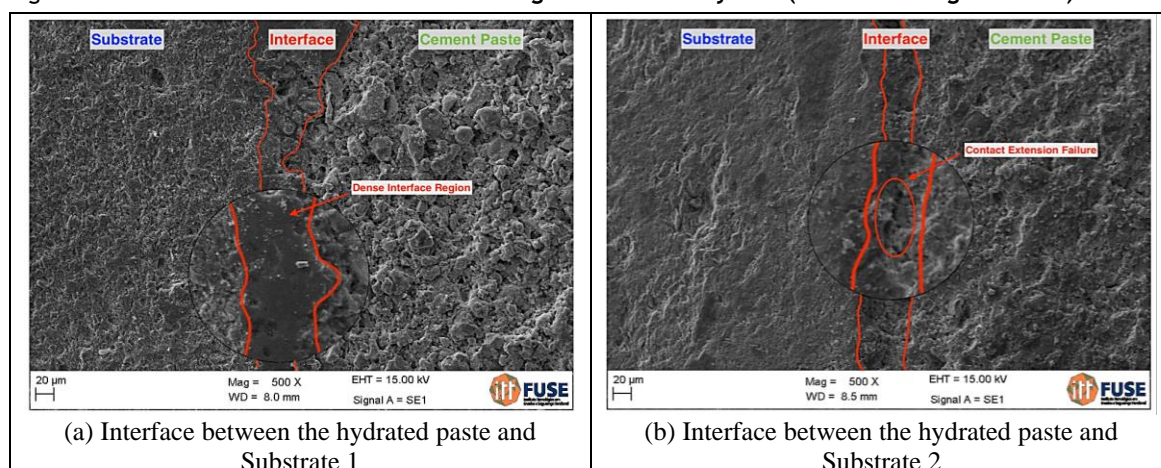
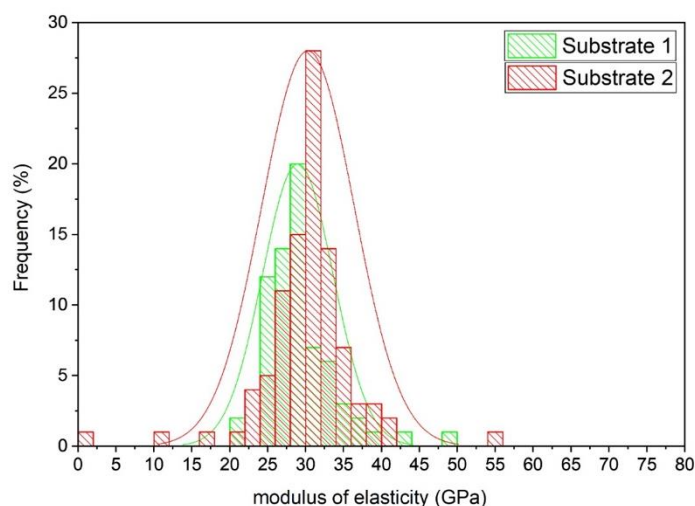


Figure 10 - Modulus of elasticity of the paste-ceramic substrate interface



The average modulus of elasticity determined in Substrates 1 and 2 were 29 GPa (SD = 4 GPa) and 30 GPa (SD = 6 GPa), respectively. The average results found from both substrates were similar, indicating that, although the characteristics of the substrates are distinct and directly influence the result of adhesive strength, on a microscale, the influence occurs less expressively. However, the standard deviation found in Substrate 2 was higher when compared to Substrate 1, indicating that the interface between the cement paste and Substrate 2 is more heterogeneous than in Substrate 1, a fact that can be related to the optical microscopy and SEM images, where failures in the contact extension can be observed, in addition to the less dense interface.

In this study, the influence of water absorption of two red ceramic substrates (with average values of $0.83 \text{ g/cm}^2 \cdot \text{h}^{1/2}$ and $0.50 \text{ g/cm}^2 \cdot \text{h}^{1/2}$) and their roughness (Ra of $1.12 \text{ }\mu\text{m}$ and $2.35 \text{ }\mu\text{m}$, respectively) on the tensile bond strength of a hydrated cement paste were evaluated.

The surface roughness of the samples extracted from the red ceramic blocks was determined in test areas with a dimension of 1 cm^2 , through a computational method that considers a cloud of points in 3 dimensions, which provides more accurate results compared to conventional methods (ARNOLD *et al.*, 2021; TONIETTO *et al.*, 2019). This same area was used for the tests of water absorption by capillarity and adhesion, reducing the error resulting from the typical heterogeneity of red ceramic surfaces (VALENTINI *et al.*, 2022).

Conclusions

The proposed methodology, in which small square areas (10 mm of edge) were established for the simultaneous determination of capillary absorption, roughness, and tensile bond strength, allows a quantitative association between the properties of the substrate and its adhesive strength, and minimises the influence of the typical heterogeneity of red ceramic surfaces in the variation of tensile bond strength.

The adoption of micro and nano-scale interface analysis techniques (optical microscopy, SEM, and AFM) allows the validation of hypotheses about the relationship between the substrate properties and the respective adhesive strength of the hydrated paste.

The capillary absorption of the substrates directly influenced the tensile bond strength as the capillary force brings the mortar grains closer to the substrate and increases the contact between the materials.

For the cement paste used, the roughness of the substrate influenced inversely proportionally the tensile bond strength. As a result, deeper valleys showed lower adhesion strengths, which suggests that the paste grains could not completely penetrate more profound valleys (due to their rheological characteristics and grain size), resulting in a loss of adhesion extension.

Analyses carried out at different scales (micro and nano scales) allow a broader understanding of the properties of materials. The optical microscopy and SEM images demonstrated that the substrate that resulted in higher tensile bond strength was the one with the densest interface region, making it possible to intuit that the higher capillary force and lower roughness allow the hydration products to better approach the surface of the substrate, resulting in a higher extent of adhesion. When reducing the evaluation scale to the nanometric level and evaluating the modulus of elasticity, it was observed that the interfaces of both substrates presented similar modulus of elasticity, however, the substrate with higher variability in the results of modulus of elasticity has lower tensile bond strength, indicating that this interface has higher porosity, which is consistent with what was observed on a macro scale.

References

- AÏT OUMEZIANE, Y. *et al.* Hygrothermal properties of an early 20th century clay brick from eastern France: Experimental characterization and numerical modelling. **Construction and Building Materials**, v. 273, p. 121763, 2021.
- AMERICAN SOCIETY FOR TESTING AND MATERIALS. **C 150/C150M**: standard specification for Portland cement. West Conshohocken, 2009.
- AMERICAN SOCIETY FOR TESTING AND MATERIALS. **C39/C39M**: standard test method for compressive strength of cylindrical concrete specimens. West Conshohocken, 2016.
- AMERICAN SOCIETY FOR TESTING AND MATERIALS. **C67**: standard test methods for sampling and testing brick and structural clay tile. West Conshohocken, 2013.
- ARNOLD, D. C. M. *et al.* A critical analysis of red ceramic blocks roughness estimation by 2d and 3d methods. **Remote Sensing**, v. 13, n. 4, p. 1–18, 2021.
- ASSOCIAÇÃO BRASILEIRA DE NORMAS TÉCNICAS. **NBR 13278**: mortars applied on walls and ceilings: determination of the specific gravity and the air entrained content in the fresh stage. Rio de Janeiro, 2005.
- ASSOCIAÇÃO BRASILEIRA DE NORMAS TÉCNICAS. **NBR 15258**: mortars applied on walls and ceilings: determination of bond tensile strength. Rio de Janeiro, 2016.
- ASSOCIAÇÃO BRASILEIRA DE NORMAS TÉCNICAS. **NBR 15270-1**: ceramic components: part 1: ceramic blocks for sealing masonry: terminology and requirements. Rio de Janeiro, 2017.
- ASSOCIAÇÃO BRASILEIRA DE NORMAS TÉCNICAS. **NBR 16606**: cement Portland: determination of normal consistency paste. Rio de Janeiro, 2018.
- ASSOCIAÇÃO BRASILEIRA DE NORMAS TÉCNICAS. **NBR 7215**: Portland cement: determination of compressive strength. Rio de Janeiro, 2019.
- ASSOCIAÇÃO BRASILEIRA DE NORMAS TÉCNICAS. **NBR 7222**: concrete and mortar: determination of tensile strength by diametral compression of cylindrical specimens. Rio de Janeiro, 2011.

- AVET, F.; LI, X.; SCRIVENER, K. Determination of the amount of reacted metakaolin in calcined clay blends. **Cement and Concrete Research**, v. 106, p. 40–48, 2018.
- AZEVEDO, A. R.G. *et al.* Influence of sintering temperature of a ceramic substrate in mortar adhesion for civil construction. **Journal of Building Engineering**, v. 19, p. 342–348, 2018.
- BARRIOS-MURIEL, J. *et al.* An approach for surface roughness filtering as an alternative to ISO standard. **Procedia Manufacturing**, v. 41, p. 674–681, 2019.
- BERNARDO, H. M. *et al.* Efeito da absorção de água e do tipo de substrato no desempenho de argamassa de revestimento nos estados fresco e endurecido. **Ambiente Construído**, Porto Alegre, v. 20, n. 3, p. 493–511, jul./set. 2020.
- BRITISH STANDARDS. **BS 3921**: specification for clay bricks. London, 1985.
- BRITISH STANDARDS. **BS EN 1015-12**: methods of test for mortar for masonry: determination of adhesive strength of hardened rendering and plastering mortars on substrates. London, 2000.
- BRITISH STANDARDS. **BS EN 771-1**: specification for masonry units: clay masonry units. London, 2011.
- CARASEK, H.; VAZ, F. H. B.; CASCUDO, O. Statistical analysis of test methods to evaluate rendering surface properties. **Ambiente Construído**, Porto Alegre, v. 18, n. 2, p. 87–105, abr./jun. 2018.
- CONSTANTINIDES, G.; ULM, F. J. The nanogranular nature of C-S-H. **Journal of the Mechanics and Physics of Solids**, v. 55, n. 1, p. 64–90, 2007.
- COSTA, E. B. C.; CARDOSO, F. A.; JOHN, V. M. Efeito do teor e da dispersão de fino calcário na aderência substrato-matriz cimentícia. **Ambiente Construído**, Porto Alegre, v. 16, n. 2, p. 21–34, abr./jun. 2016.
- COSTA, E. B. C.; CARDOSO, F. A.; JOHN, V. M. Influence of high contents of limestone fines on rheological behaviour and bond strength of cement-based mortars. **Construction and Building Materials**, v. 156, p. 1114–1126, 2017.
- COUTO CARNEIRO, A. M.; PINTO CARVALHO, R.; ANDRADE PIRES, F. M. Representative contact element size determination for micromechanical contact analysis of self-affine topographies. **International Journal of Solids and Structures**, v. 206, p. 262–281, 2020.
- CULTRONE, G. *et al.* Influence of mineralogy and firing temperature on the porosity of bricks. **Journal of the European Ceramic Society**, v. 24, n. 3, p. 547–564, 2004.
- DETRICHE, C. H. *et al.* Influence des paramètres de mise en œuvre et de composition sur le comportement des mortiers d'enduit. **Materials and Structures**, v. 18, n. 3, p. 193–200, 1985.
- DUPIN, I.; DETRICHE, C. H.; MASO, J. C. Accrochage direct d'un enduit sur un isolant par une liaison de type mécanique dans le cadre d'un procédé d'isolation par l'extérieur. **Materials and Structures**, v. 21, n. 5, p. 370–378, 1988.
- FOUCHAL, F.; LEBON, F.; TITEUX, I. Contribution to the modelling of interfaces in masonry construction. **Construction and Building Materials**, v. 23, n. 6, p. 2428–2441, 2009.
- GONZÁLEZ-SÁNCHEZ, J. F. *et al.* Improving lime-based rendering mortars with admixtures. **Construction and Building Materials**, v. 271, 2021.
- GROOT, C.; LARBI, J. Influence of water flow (reversal) on bond strength development in young masonry. **Heron**, v. 44, n. 2, p. 63–78, 1999.
- HAN, J. *et al.* Microstructure Modification of Carbonated Cement Paste with Six Kinds of Modern Microscopic Instruments. **Journal of Materials in Civil Engineering**, v. 27, n. 10, p. 04014262, 2015.
- HOŁA, J. *et al.* Usefulness of 3D surface roughness parameters for nondestructive evaluation of pull-off adhesion of concrete layers. **Construction and Building Materials**, v. 84, p. 111–120, 2015.
- HUANG, Q. *et al.* Recycling of crushed waste clay brick as aggregates in cement mortars: An approach from macro- and micro-scale investigation. **Construction and Building Materials**, v. 274, p. 122068, 2021.
- KAHANGI SHAHREZA, S.; NIKLEWSKI, J.; MOLNÁR, M. Experimental investigation of water absorption and penetration in clay brick masonry under simulated uniform water spray exposure. **Journal of Building Engineering**, v. 43, 2021.

- KAZMIERCZAK, C. de S.; ROSA, M.; ARNOLD, D. C. M. Influência da adição de filer de areia de britagem nas propriedades de argamassas de revestimento. **Ambiente Construído**, Porto Alegre, v. 16, n. 2, p. 7–19, abr./jun. 2016.
- KENDALL, K. **Molecular adhesion and its applications**. New York: Kluwer Academic Publishers, 2001. v. 53.
- KOZUBAL, J. *et al.* Non-deterministic assessment of surface roughness as bond strength parameters between concrete layers cast at different ages. **Materials**, v. 13, n. 11, 2020.
- LI, X. *et al.* Effect of surface roughness on capillary force during particle-wall impaction under different humidity conditions. **Powder Technology**, v. 371, p. 244–255, 2020.
- MONTEIRO, P. J. M.; MASO, J. C.; OLLIVIER, J. P. Particle size analysis of the sand. **Cement and Concrete Research**, v. 15, n. c, p. 953–958, 1985.
- PAES, I. N. *et al.* Influence of water transportation inside a mortar/block system on bonding resistance behavior. **Revista Ingeniería de Construcción**, v. 29, n. 2, p. 175–186, 2014.
- PALOMAR, I.; BARLUENGA, G. A multiscale model for pervious lime-cement mortar with perlite and cellulose fibers. **Construction and Building Materials**, v. 160, p. 136–144, 2018.
- PINHEIRO, B. C. A.; HOLANDA, J. N. F. Efeito da temperatura de queima em algumas propriedades mecânicas de cerâmica vermelha. **Cerâmica**, v. 56, n. 339, p. 237–243, 2010.
- RAMIREZ, R. *et al.* Experimental characterization of moisture transport in brick masonry with natural hydraulic lime mortar. **Building and Environment**, v. 205, p. 108256, 2021.
- RAUCCI, J. S. *et al.* Efeito do método de mistura sobre o espalhamento mini-slump de pastas de cimento Portland. **RIEM - IBRACON Structures and Materials Journal**, v. 11, n. 2, 2018.
- SANJAY, S. L. *et al.* Recent progress in preparation of superhydrophobic surfaces: a review. **Journal of Surface Engineered Materials and Advanced Technology**, v. 2, p. 76–94, 2012.
- SANTOS, A. R. L. *et al.* Tensile bond strength of lime-based mortars: the role of the microstructure on their performance assessed by a new non-standard test method. **Journal of Building Engineering**, v. 29, 2020.
- SARKER, M.; DIAS-DA-COSTA, D.; HADIGHEH, S. A. Multi-scale 3D roughness quantification of concrete interfaces and pavement surfaces with a single-camera set-up. **Construction and Building Materials**, v. 222, p. 511–521, 2019.
- SENTENA, J. A. A.; KAZMIERCZAK, C. S.; KREIN, L. A. Degradação de revestimentos de argamassa com finos de resíduos de concreto por ciclos térmicos. **Ambiente Construído**, Porto Alegre, v. 18, n. 1, p. 211–224, jan./mar. 2018.
- SHULTZ, J.; NARDIN, M. Theories and mechanisms of adhesion. *In*: PIZZI, A.; MITTAL, K. L. **Handbook of adhesive technology**. New York: Marcell Dekker Inc, 2003. Cap 3.
- SORELLI, L. *et al.* The nano-mechanical signature of Ultra High Performance Concrete by statistical nanoindentation techniques. **Cement and Concrete Research**, v. 38, n. 12, p. 1447–1456, 2008.
- STOLZ, C. M.; MASUERO, A. B. Influence of grains distribution on the rheological behavior of mortars. **Construction and Building Materials**, v. 177, p. 261–271, 2018.
- THAMBOO, J. A.; DHANASEKAR, M. Characterisation of thin layer polymer cement mortared concrete masonry bond. **Construction and Building Materials**, v. 82, p. 71–80, 2015.
- THORNTON, C.; CUMMINS, S. J.; CLEARY, P. W. On elastic-plastic normal contact force models, with and without adhesion. **Powder Technology**, v. 315, p. 339–346, 2017.
- TONIETTO, L. *et al.* Method for evaluating roughness and valley areas coefficients of surfaces acquired by laser scanner. **Scientific Reports**, v. 12, n. 1, 2022.
- TONIETTO, L. *et al.* New method for evaluating surface roughness parameters acquired by laser scanning. **Scientific Reports**, v. 9, n. 1, p. 1–16, 2019.
- TORRES, I.; VEIGA, R.; FREITAS, V. Influence of substrate characteristics on behavior of applied mortar. **Journal of Materials in Civil Engineering**, v. 30, n. 10, p. 1–13, 2018.

VALENTINI, P. *et al.* Methodology for evaluation of the influence of roughness and capillary absorption of ceramic blocks on the render's tensile bond strength. **Cerâmica**, v. 68, 2022.

VALENTINI, P. **Influence of water absorption and roughness of ceramic substrates and filler addition on adherence of coating mortars**. São Leopoldo, 2018. 145 f. Mestrado em Engenharia Civil – Programa de Pós-Graduação em Engenharia Civil. Universidade do Vale do Rio dos Sinos, 2018.

VAN DAM, J. P. B. *et al.* Effect of surface roughness and chemistry on the adhesion and durability of a steel-epoxy adhesive interface. **International Journal of Adhesion and Adhesives**, v. 96, p. 102450, 2020.

VAZ, F. H. B.; CARASEK, H. Resistência de aderência de revestimentos de argamassa: contribuição por meio de mapeamento e revisão sistemática de literatura para futuras pesquisas no tema. **Cerâmica**, v. 65, p. 303–318, 2019.

VENKATARAMA REDDY, B. V.; LAL, R.; NANJUNDA RAO, K. S. Enhancing bond strength and characteristics of soil-cement block masonry. **Journal of Materials in Civil Engineering**, v. 19, n. 2, p. 164–172, 2007.

VERPLANCK, N. *et al.* Wettability switching techniques on superhydrophobic surfaces. **Nanoscale Research Letters**, v. 2, n. 12, p. 577–596, 2007.

WANG, H. *et al.* The effects of leaf roughness, surface free energy and work of adhesion on leaf water drop adhesion. **PLoS ONE**, v. 9, n. 9, 2014.

WILSON, M. A.; CARTER, M. A.; HOFF, W. D. British Standard and RILEM water absorption tests: A critical evaluation. **Materials and Structures/Materiaux et Constructions**, v. 32, n. 8, p. 571–578, 1999.

YANG, C.; PERSSON, B. N. J. Contact mechanics: Contact area and interfacial separation from small contact to full contact. **Journal of Physics Condensed Matter**, v. 20, 2008.

ZANELATO, E. B. *et al.* Evaluation of roughcast on the adhesion mechanisms of mortars on ceramic substrates. **Materials and Structures/Materiaux et Constructions**, v. 52, n. 3, 2019.

ZUO, S.; XIAO, J.; YUAN, Q. Comparative study on the new-old mortar interface deterioration after wet-dry cycles and heat-cool cycles. **Construction and Building Materials**, v. 244, p. 118374, 2020.

Camila Werner Menegotto

Conceptualization, Methodology, Formal analysis, Investigation, Writing - original draft, Writing and editing.

Graduation Program in Civil Engineering | Universidade do Vale do Rio dos Sinos | Av. Unisinos, 950, Cristo Rei | São Leopoldo - RS - Brasil | Tel.: +55 (51) 3590-8766 | E-mail: camila-wm@hotmail.com

Monique Palavro Lunardi

Methodology, Formal analysis, Writing - original draft, Writing and editing.

Graduation Program in Civil Engineering | Universidade do Vale do Rio dos Sinos | E-mail: monique.lunardi@lme.pcc.usp.br

Daiana Metz Arnold

Writing - review & editing.

Graduation Program in Civil Engineering | Universidade Feevale | ERS-239, 2755 | Novo Hamburgo - RS - Brasil | CEP 93525-075 | Tel.: +55 (51) 3586-8800 | E-mail: daim@feevale.br

Leandro Tonietto

Methodology, Writing - review & editing, Data processing

Graduation Program in Applied Computing | Universidade do Vale do Rio dos Sinos | Av. Unisinos, 950, Cristo Rei | São Leopoldo - RS - Brasil | Tel.: +55 (51) 3590-8766 | E-mail: ltonietto@unisinos.br

Valéria Costa de Oliveira

Conceptualization.

Civil Engineering Coordination | Instituto Federal de Educação, Ciência e Tecnologia | Av. Calama, 4985 | Porto Velho - RO - Brazil | CEP 76820-441 | E-mail: valeria.oliveira@ifro.edu.br

Marlova Piva Kulakowski

Writing - review & editing.

Graduation Program in Civil Engineering | Universidade do Vale do Rio dos Sinos | E-mail: marlovak@unisinos.br

Claudio de Souza Kazmierczak

Conceptualization, Methodology, Supervision, Writing - review & editing.

Graduation Program in Civil Engineering | Universidade do Vale do Rio dos Sinos | E-mail: claudiok@unisinos.br

Editor do artigo: **Marcelo Henrique Farias de Medeiros**

Editores de seção: **Ercília Hitomi Hirota e Juliana Parise Baldauf**

Ambiente Construído

Revista da Associação Nacional de Tecnologia do Ambiente Construído

Av. Osvaldo Aranha, 99 - 3º andar, Centro

Porto Alegre - RS - Brasil

CEP 90035-190

Telefone: +55 (51) 3308-4084

www.seer.ufrgs.br/ambienteconstruido

www.scielo.br/ac

E-mail: ambienteconstruido@ufrgs.br



This is an open-access article distributed under the terms of the Creative Commons Attribution License.